Genetic, clinical underpinnings of subtle early brain change along Alzheimer's dimensions

Junhao Wen[1*], Zhijian Yang[1], Ilya M. Nasrallah[1], Yuhan Cui[1], Guray Erus[1], Dhivya Srinivasan[1], Ahmed Abdulkadir[1,2], Elizabeth Mamourian[1], Gyujoon Hwang[1], Ashish Singh[1], Mark Bergman[1], Jingxuan Bao[3], Erdem Varol[4], Zhen Zhou[1], Aleix Boquet-Pujadas[5], Jiong Chen[1], Arthur Toga[6], Andrew J. Saykin[7], Timothy J. Hohman[8], Paul M. Thompson[9], Sylvia Villeneuve[10], Randy Gollub[11], Aristeidis Sotiras[12], Katharina Wittfeld[13,14], Hans J. Grabe[13,14], Duygu Tosun[15], Murat Bilgel[16], Yang An[16], Daniel S. Marcus[17], Pamela LaMontagne[17], Susan R. Heckbert[18], Thomas R. Austin[18], Lenore J. Launer[19], Mark Espeland[20], Colin L Masters[21], Paul Maruff[21], Jurgen Fripp[22], Sterling C. Johnson[23], John C. Morris[24], Marilyn S. Albert[25], R. Nick Bryan[26], Susan M. Resnick[16], Luigi Ferrucci[27], Yong Fan[1], Mohamad Habes[28], David Wolk[1, 29], Li Shen[3], Haochang Shou[1,30], Christos Davatzikos[1*]

[1]Artificial Intelligence in Biomedical Imaging Laboratory (AIBIL), Center for AI and Data Science for Integrated Diagnostics (AI[2]D), Perelman School of Medicine, University of Pennsylvania, Philadelphia, USA.
[2]Research Lab in Neuro-imaging of the Department of Clinical Neurosciences at Lausanne University Hospital, Lausanne, Switzerland
[3]Department of Biostatistics, Epidemiology and Informatics University of Pennsylvania Perelman School of Medicine, Philadelphia, USA
[4]Department of Statistics, Center for Theoretical Neuroscience, Zuckerman Institute, Columbia University, New York, New York
[5]Biomedical Imaging Group, EPFL, Lausanne, Switzerland
[6]Laboratory of Neuro Imaging, Stevens Neuroimaging and Informatics Institute, Keck School of Medicine of USC, University of Southern California, Marina del Rey, California
[7]Radiology and Imaging Sciences, Center for Neuroimaging, Department of Radiology and Imaging Sciences, Indiana Alzheimer's Disease Research Center and the Melvin and Bren Simon Cancer Center, Indiana University School of Medicine, Indianapolis
[8]Vanderbilt Memory and Alzheimer's Center, Vanderbilt Genetics Institute, Department of Neurology, Vanderbilt University Medical Center, Nashville, TN USA
[9]Imaging Genetics Center, Mark and Mary Stevens Neuroimaging and Informatics Institute, Keck School of Medicine of USC, University of Southern California, Marina del Rey, California
[10]Douglas Mental Health University Institute, McGill University, Montréal, Québec, Canada
[11]Athinoula A. Martinos Center for Biomedical Imaging, Massachusetts General Hospital, Harvard Medical School, Charlestown, Massachusetts
[12]Department of Radiology and Institute for Informatics, Washington University School of Medicine, St. Louis, USA
[13]German Center for Neurodegenerative Diseases (DZNE), Site Rostock/ Greifswald, Greifswald, Germany
[14]Department of Psychiatry and Psychotherapy, University Medicine Greifswald, Greifswald, Germany
[15]Department of Radiology and Biomedical Imaging, University of California, San Francisco, CA, USA
[16]Laboratory of Behavioral Neuroscience, National Institute on Aging, NIH, USA
[17]Department of Radiology, Washington University School of Medicine, St. Louis, Missouri, USA
[18]Cardiovascular Health Research Unit and Department of Epidemiology, University of Washington, Seattle, WA, USA
[19]Neuroepidemiology Section, Intramural Research Program, National Institute on Aging, Bethesda, Maryland, USA
[20]Sticht Center for Healthy Aging and Alzheimer's Prevention, Wake Forest School of Medicine, Winston-Salem, North Carolina, USA
[21]Florey Institute of Neuroscience and Mental Health, The University of Melbourne, Parkville, VIC, Australia
[22]CSIRO Health and Biosecurity, Australian e-Health Research Centre CSIRO, Brisbane, Queensland, Australia
[23]Wisconsin Alzheimer's Institute, University of Wisconsin School of Medicine and Public Health, Madison, Wisconsin, USA
[24]Knight Alzheimer Disease Research Center, Washington University in St. Louis, St. Louis, MO, USA
[25]Department of Neurology, Johns Hopkins University School of Medicine, USA
[26]Department of Radiology, University of Pennsylvania, Philadelphia, USA.

[27]Translational Gerontology Branch, Longitudinal Studies Section, National Institute on Aging, National Institutes of Health, MedStar Harbor Hospital, 3001 S. Hanover Street, Baltimore, MD, 21225, USA
[28]Glenn Biggs Institute for Alzheimer's & Neurodegenerative Diseases, University of Texas Health Science Center at San Antonio, San Antonio, USA
[29]Department of Neurology and Penn Memory Center, University of Pennsylvania, Philadelphia, USA
[30]Penn Statistics in Imaging and Visualization Center, Department of Biostatistics, Epidemiology, and Informatics, Perelman School of Medicine, University of Pennsylvania, Philadelphia, USA

[*]Corresponding authors:
Junhao Wen, Ph.D. – junhao.wen89@gmail.com
Christos Davatzikos, Ph.D. – Christos.Davatzikos@pennmedicine.upenn.edu
3700 Hamilton Walk, 7th Floor, Philadelphia, PA 19104

eMethod 1: Surreal-GAN: methodological considerations and advances

Surreal-GAN[1] is a novel deep representation learning method proposed for dissecting disease-related neuroanatomical heterogeneity from imaging data. Compared to its precursor, the Smile-GAN model,[2] Surreal-GAN follows the same principle of semi-supervised clustering but solves several limitations of Smile-GAN. Semi-supervised clustering methods seek the so-called "*1-to-k*" mapping by learning distribution transformation from cognitively unimpaired (CU) data to patient (PT) data. The following schematic figure demonstrates the principles of Smile-GAN and Surreal-GAN in the semi-supervised learning framework to disentangle AD neuroanatomical heterogeneity.

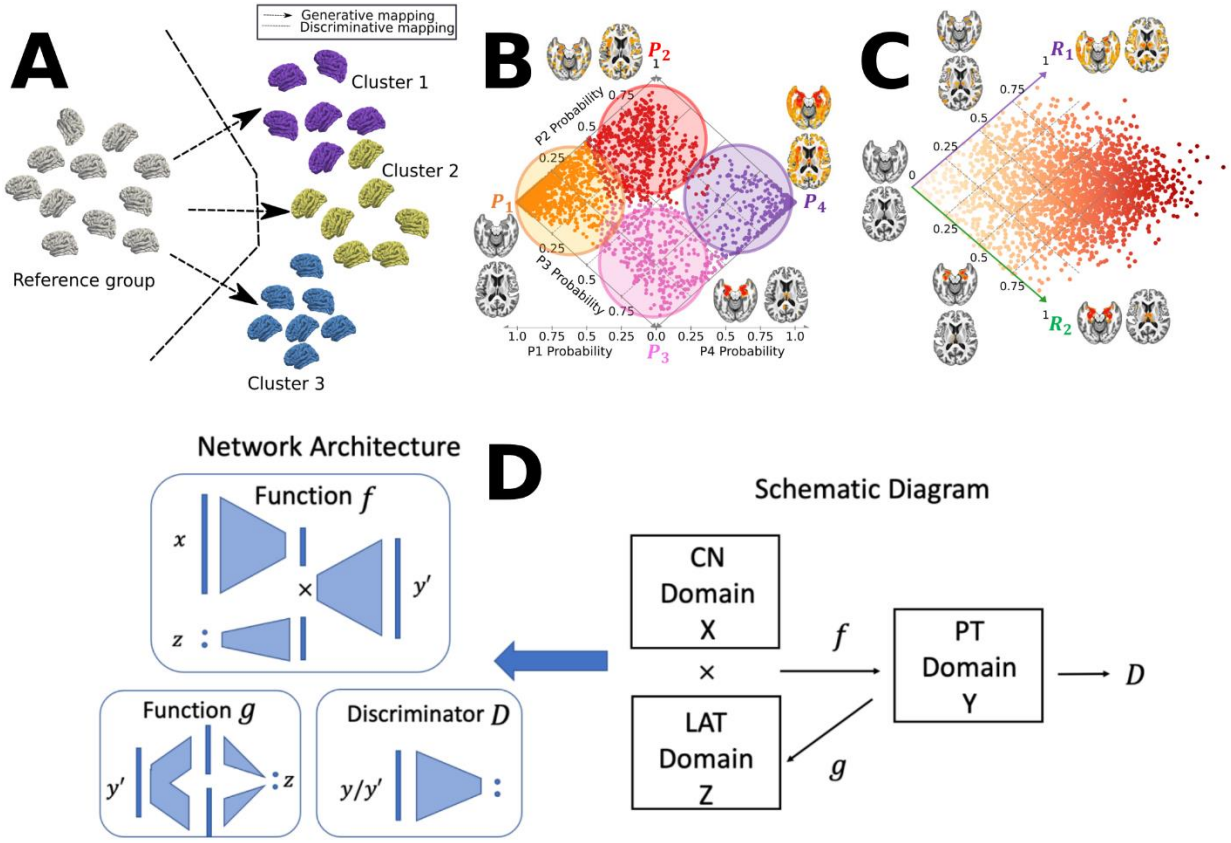

Fig. **A**) Schematic figures of semi-supervised clustering methods, including generative[1–3] and discriminative approaches.[4,5] Semi-supervised clustering methods dissect the neuroanatomical heterogeneity of brain diseases by seeking the so-called "*1-to-k*" mapping between the healthy control (CN) group as a reference and the patient (PT) group as a target. They sought to tease out clusters that are likely driven by distinct pathological trajectories instead of by global similarity/dissimilarity in data. The figure is adapted from our previous work.[6] **B**) Conceptual illustration of applying Smile-GAN ADNI to cluster MCI/AD participants into four hard-coded subtypes (P1, P2, P3, and P4) and two longitudinal pathways after applying the model to longitudinal data: P1→P2→P4; *ii*) P1→P3→P4. The figure is adapted from our previous work.[2] **C**) Conceptual illustration of applying Surreal-GAN to ADNI to recapitulate the

neuroanatomical heterogeneity of MCI/AD participants into two continuous dimensional scores. Methodological advances are to capture disease severity and heterogeneity simultaneously using only cross-sectional data and allow the same individuals to express themselves along multiple dimensions. The figure is adapted from our previous work.[1] **D**) General network architectures (left) and schematic diagram of the semi-supervised learning (right, corresponding to Fig. A). The figure is adapted from our previous work.[1]

Smile-GAN learns one transformation function, *f*, which generates synthesized PT data, $\boldsymbol{y}' = f(\boldsymbol{x}, \boldsymbol{z})$, from real CU data $\boldsymbol{x}$ and the latent variable $\boldsymbol{z}$**.** The categorical variable $\boldsymbol{z}$ is encoded as an *M*-dimensional one-hot vector with value 1 being placed at any position with equal probability (i.e., *1/k*). Thus, *k* different values of $\boldsymbol{z}$ lead to *k* different mapping directions and enable *M* subgroups clustering.

Surreal-GAN also learns one transformation function f, which transforms CU data $\boldsymbol{x}$ to different synthesized PT data $\boldsymbol{y}' = f(\boldsymbol{x}, \boldsymbol{z})$, with latent variable $\boldsymbol{z}$ specifying distinct mapping directions. However, compared to Smile-GAN, Surreal-GAN considers that disease heterogeneity spatially and temporally (subtype) expands along a continuum (severity), similar to Sustain[7] to a certain extent. Thus, the latent variable $\boldsymbol{z}$ is modeled as a continuous variable, allowing infinite mapping directions from CU to PT data. $\boldsymbol{z} \sim p_{lat}(\boldsymbol{z})$ is sampled from a multivariate uniform distribution $U(0,1)^k$, rather than a categorical distribution as in Smile-GAN. Further, Surreal-GAN aims at disentangling spatial and temporal variations independently so that each dimension of the latent variable $\boldsymbol{z}$ is correlated with the severity of one relatively homogeneous imaging pattern. In contrast, different dimensions can be associated with spatially different imaging patterns.

To achieve the goals above, the objective function of Surreal-GAN consists of one adversarial loss and other regularization terms. The adversarial loss aims at matching the distribution of synthesized PT data, p_{syn}, and the distribution of real PT data, p_{PT}. Other regularization terms serve the following purposes: 1) encouraging sparse transformations (change loss); 2) reconstructing latent variables from synthesized or real PT data through the decomposer g_1 (decomposition loss) and reconstruction function g_2 (reconstruction loss); 3) boosting spatial separation of synthesized/captured patterns (orthogonality loss); 4) enforcing positive correlations between components of $\boldsymbol{z}$ and severity of synthesized patterns (monotonicity loss and cn loss).

Specifically, with distributions of CU, real PT, synthesized PT data denoted as $p_{CU}(\boldsymbol{x})$, $p_{PT}(\boldsymbol{y})$ and $p_{syn}(\boldsymbol{y}')$ respectively, the adversarial loss is defined as:

$$L_{GAN}(D,f) = E_{\boldsymbol{y}\sim p_{PT}(\boldsymbol{y})}\left[log\left(D(\boldsymbol{y})\right)\right] + E_{\boldsymbol{z}\sim p_{Lat}(\boldsymbol{z}),\boldsymbol{x}\sim p_{CN}(\boldsymbol{x})}\left[1 - log\left(D\left(f(\boldsymbol{x},\boldsymbol{z})\right)\right)\right]$$

$$= E_{\boldsymbol{y}\sim p_{PT}(\boldsymbol{y})}\left[log\left(D(\boldsymbol{y})\right)\right] + E_{p_{syn}(\boldsymbol{y}')}\left[1 - log\left(D(\boldsymbol{y}')\right)\right]$$

The transformation function attempts to synthesize PT data $\boldsymbol{y}'$, so that they follow similar distributions as real PT data. The discriminator, D, tries to distinguish the synthesized PT data from real PT data. Therefore, the discriminator is updated to maximize the adversarial loss, while the transformation function is optimized to minimize it.

Other regularization terms are introduced to further regularize the transformation function f. With the assumption that the disease process will not change brain anatomy dramatically and primarily only affect certain regions throughout most of the disease stages, the change loss is introduced to control sparsity and distance of transformations:

$$L_{change}(f) = E_{\boldsymbol{z}\sim p_{Lat}(\boldsymbol{z}),\boldsymbol{x}\sim p_{CU}(\boldsymbol{x})}[\|f(\boldsymbol{x},\boldsymbol{z}) - \boldsymbol{x}\|_1]$$

The decomposer g_1 serves to reconstruct changes synthesized by each component: $\boldsymbol{q}_i = f(\boldsymbol{x},\boldsymbol{a}^i) - \boldsymbol{x}$, where $\boldsymbol{a}_i^i = \boldsymbol{z}_i$ and $\boldsymbol{a}_j^i = 0$ for $j \neq i$. With $\widehat{\boldsymbol{q}}_{f(x,z)} = [\boldsymbol{q}_1^T, \boldsymbol{q}_2^T, \cdots, \boldsymbol{q}_M^T]^T$, the decomposition loss is defined as:

$$L_{decom}(f, g_1) = E_{\boldsymbol{z}\sim p_{Lat}(\boldsymbol{z}),\boldsymbol{x}\sim p_{CN}(\boldsymbol{x})}\left[\left\|g_1(f(\boldsymbol{x},\boldsymbol{z})) - \widehat{\boldsymbol{q}}_{f(\boldsymbol{x},\boldsymbol{z})}\right\|_2\right]$$

The reconstruction function g_2 serves to further reconstruct each component of the sampled $\boldsymbol{z}$ variable from $g_1\left(f(\boldsymbol{x},\boldsymbol{z})\right)$. The function g is defined as a composition of g_1 and g_2, with $g\left(f(\boldsymbol{x},\boldsymbol{z})\right) = \left[g_2\left(g_1\left(f(\boldsymbol{x},\boldsymbol{z})\right)_{0:S}\right), \cdots, g_2\left(g_1\left(f(\boldsymbol{x},\boldsymbol{z})\right)_{S*(M-1):S*M}\right)\right]^T$ (S = number of ROIs), and the reconstruction loss is defined as

$$L_{recons}(f, g) = L_{recons}(f, g_1, g_2) = E_{\boldsymbol{z}\sim p_{Lat}(\boldsymbol{z}),\boldsymbol{x}\sim p_{CN}(\boldsymbol{x})}\left[\left\|g\left(f(\boldsymbol{x},\boldsymbol{z})\right) - \boldsymbol{z}\right\|_2\right]$$

The orthogonality loss aims to boost changes led each component, $\boldsymbol{q}_i$, to be relatively orthogonal to each other. For this purpose, a matrix $\boldsymbol{A}_{f(\boldsymbol{x},\boldsymbol{z})}$ *i*s constructed with the i_{th} column $A_{f(\boldsymbol{x},\boldsymbol{z})_{:,i}} = \boldsymbol{q}_i/||\boldsymbol{q}_i||_2$, and the orthogonality loss is defined as:

$$L_{ortho}(f) = E_{\boldsymbol{z}\sim p_{Lat}(z),\boldsymbol{x}\sim p_{CU}(\boldsymbol{x})}[||\boldsymbol{A}_{f(\boldsymbol{x},\boldsymbol{z})}^T\boldsymbol{A}_{f(\boldsymbol{x},\boldsymbol{z})} - I||_F]$$

To encourage a positive correlation between the severity of the synthesized pattern and the value of each component $\boldsymbol{z}_i$, another latent variable $\boldsymbol{z}' \sim p_{sev}(\boldsymbol{z}'|\boldsymbol{z})$ is sampled conditioned on previously sampled $\boldsymbol{z}$ variables, such that $\boldsymbol{z}'_i \geq \boldsymbol{z}_i$ for any $1 \leq i \leq k$. With these two sampled latent variables, the monotonicity loss is defined as:

$$L_{mono}(f) = E_{\boldsymbol{z}\sim p_{Lat}(\boldsymbol{z}),\boldsymbol{z}\sim p_{sev}(\boldsymbol{z}'|\boldsymbol{z}),\boldsymbol{x}\sim p_{CU}(\boldsymbol{x})}[||max(|f(\boldsymbol{x},\boldsymbol{z}) - \boldsymbol{x}| - |f(\boldsymbol{x},\boldsymbol{z}') - \boldsymbol{x}|,0)||_2]$$

The cn loss is introduced to further ensure that a small $\boldsymbol{z}$ variable lead to mild patterns. By letting $p_{cn}(\boldsymbol{z}) = U(0,0.05)^k$ to be a multivariate uniform distribution, the cn loss is defined as:

$$L_{cn}(f) = E_{\boldsymbol{z^{cn}}\sim p_{cn}(\boldsymbol{z}),\boldsymbol{x}\sim p_{CU}(\boldsymbol{x})}[\|f(\boldsymbol{x},\boldsymbol{z^{cn}}) - \boldsymbol{x}\|_1]$$

With all loss functions introduced above, the full objective of Surreal-GAN can be written as

$$L(D,f,g_1,g_2) = L_{GAN}(D,f) + \gamma L_{change}(f) + \kappa L_{decom}(f,g_1) + \zeta L_{recon}(f,g_1,g_2) + \lambda L_{ortho}(f) + \mu L_{mono}(f) + \eta L_{cn}(f)$$

With γ, κ, ζ, λ, μ, and η being hyperparameters that control the relative importance of each loss function during the training process. More details of parameter selections can be found in the Surreal-GAN paper.[1]

Through the training process, parametrized functions f , $g_{1,}$ and g_2 are updated to satisfy that:

$$f, g_1, g_2 = arg \min_{f,g} \max_{D} L(D,f,g_1,g_2)$$

More importantly, after the training process, the function g, a composition of g_1 and g_2, can be applied to unseen PT data to infer the latent variable, which is referred to as the R-indices (i.e., dimensions) of PT data.

eMethod 2: Image quality check

Raw T1-weighted MRIs were first quality checked (QC) for motion, image artifacts, or restricted field-of-view. Another QC was performed as follows: First, the images were examined by manually evaluating for pipeline failures (e.g., poor brain extraction, tissue segmentation, and registration errors). Furthermore, a second step automatically flagged images based on outlying values of quantified metrics (i.e., PSC values); those flagged images were re-evaluated.

eFigure 1: The age distribution of the four populations and the expression of the R1 and R2 dimensions

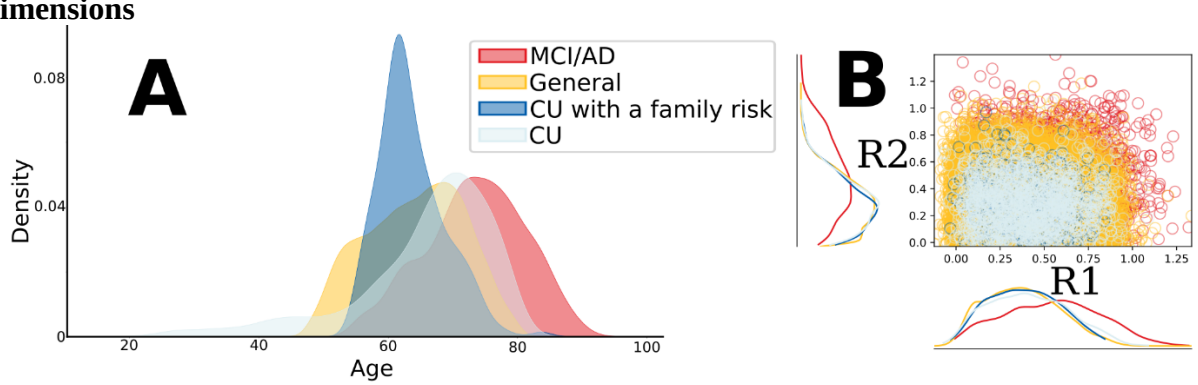

A) Four different populations were used in this study: *i*) the *MCI/AD population* from ADNI[8] and BLSA,[9] which represented the symptomatic population (age distribution: 73.45±7.69); *ii*) the *general population* from UKBB,[10] which included participants with high AD risks based on family history of AD (i.e., proxy-AD, *N*=10,189 out of 39,575) and many other disease diagnoses (age distribution: 64.12±7.54); *iii*) the *cognitively unimpaired (CU) population* from ADNI[8] and BLSA,[9] which endorsed the normative aging elders without any cognitive decline at baseline (age distribution: 65.75±10.90); *iv*) the *CU with a family risk population*, which recruited 343 CU participants that had a first-relative family history of AD diagnosis (age distribution: 63.62±5.05). Refer to Method 1 in the main manuscript for more details. A kernel density estimate plot visualizes the age distribution of each population. **B**) The scatter plot for the R1 and R2 dimensions in the four populations is presented, together with the kernel density estimate plot for each population. The two dimensions are highly expressed in the MCI/AD population and gradually less manifested in the three asymptomatic populations: the general population, the CU population, and the CU with a family history population. Of note, some participants showed negative values for the two neuroanatomical dimensions. These participants did not express much for this dimension and can be interpreted as super normal individuals compared to the MCI/AD patients from ADNI in the training sample.

eFigure 2: PRS plots at baseline for the MCI/AD population

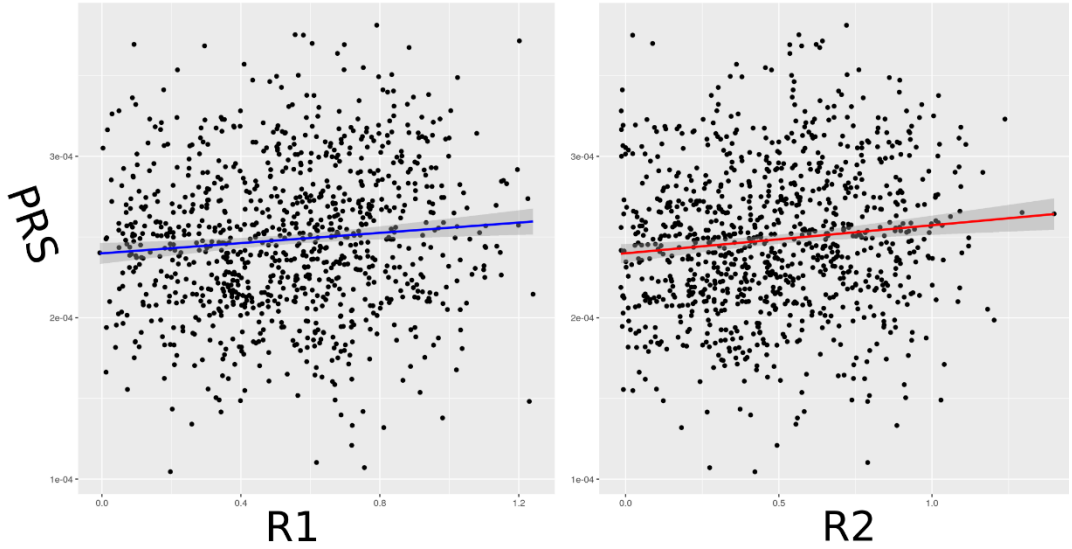

We fit a linear regression model to associate the PRS with the two dimensions (**Method 6F** in the main manuscript). The results showed a slightly stronger positive association with the R2 dimension [r=0.11, -$\log_{10}$(P-value)=3.14] than with the R1 dimension [r=0.09, -$\log_{10}$(P-value)=2.31].

eFigure 3: QQ plots for the baseline GWAS for the MCI/AD population

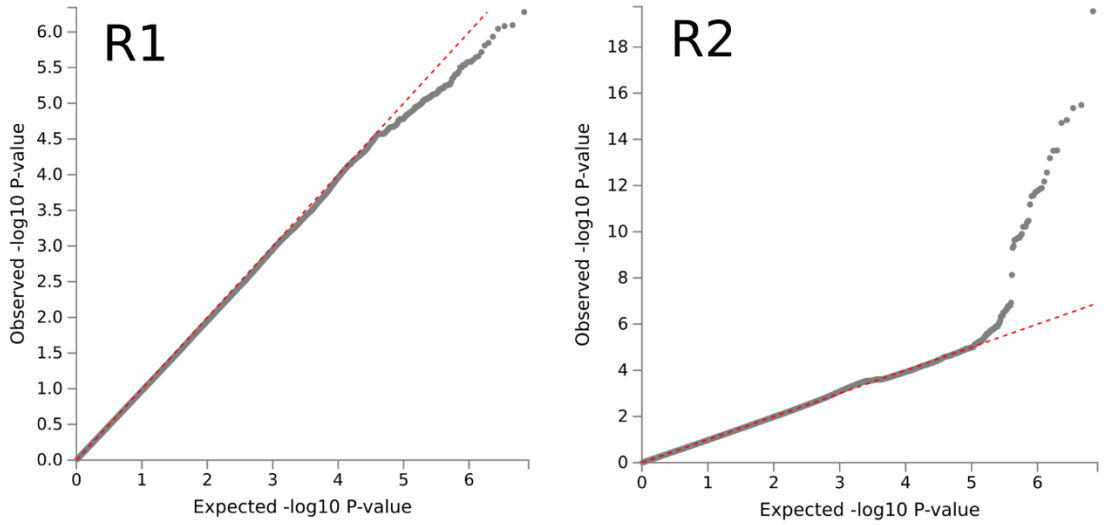

The FUMA online platform generates the QQ plot of the two GWAS for the R1 and R2 neuroanatomical dimensions.

eFigure 4: QQ plots for the longitudinal GWAS for the general population

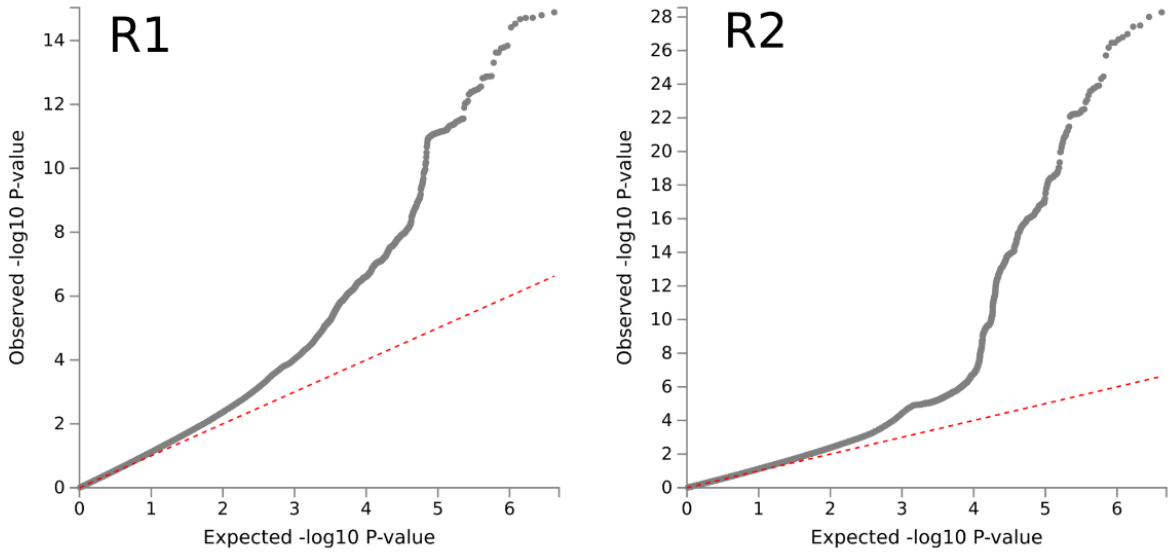

The FUMA online platform generates the QQ plot of the two GWAS for the R1 and R2 neuroanatomical dimensions.

eFigure 5: Tissue specificity analyses for the prioritized genes in the two dimensions in the general population

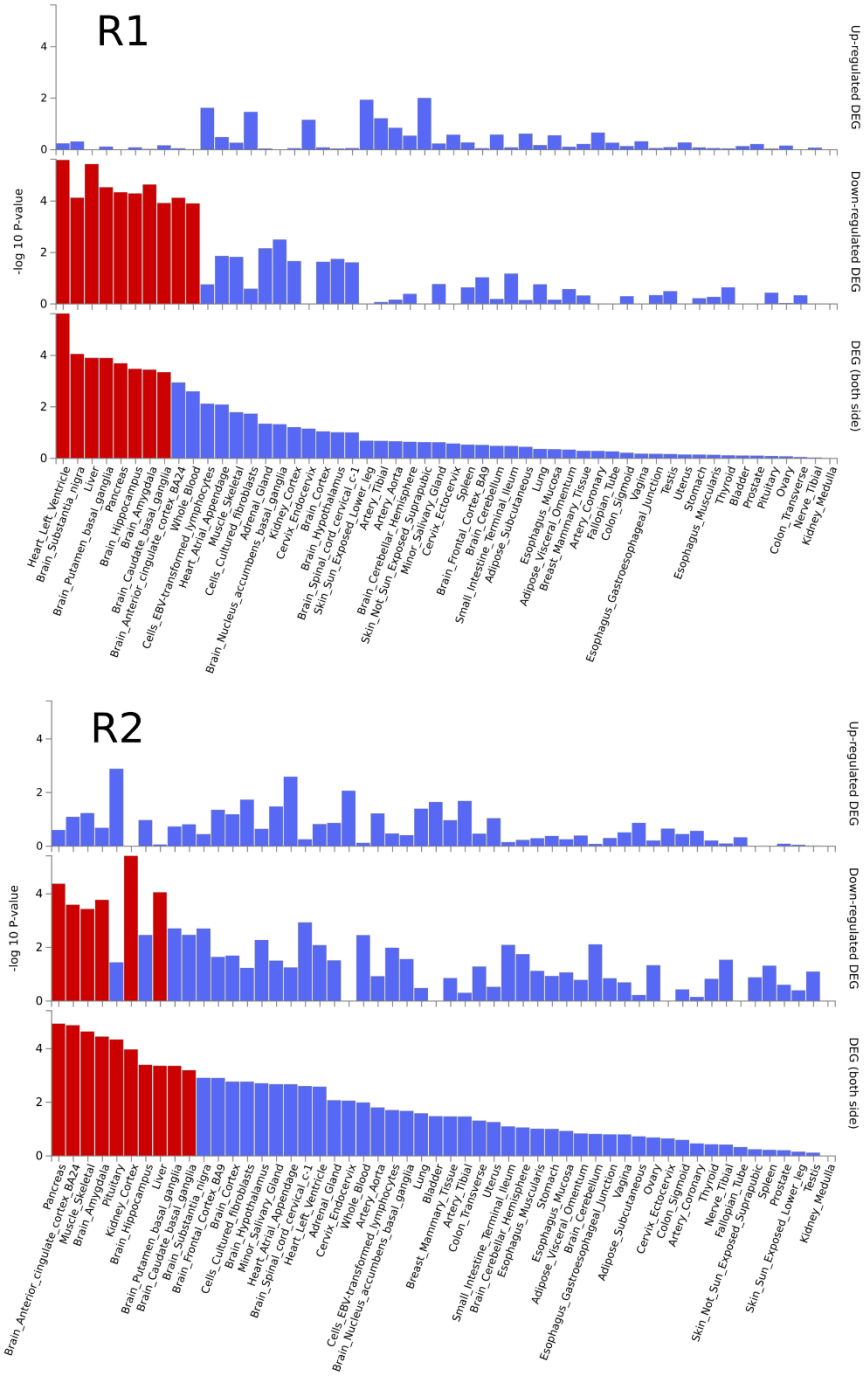

We performed a prioritized tissue specificity analysis using the mapped/annotated genes. Significantly enriched differentially expressed gene sets (DEG) are highlighted in red. The *GENE2FUNC*[11] pipeline from FUMA was performed to examine the overrepresentation of prioritized genes in pre-defined DEGs (up-regulated, down-regulated, and both-side DEGs) from different gene expression data. The input genes (Fig. 2C) were tested against each DEG using the hypergeometric test.

eFigure 6: Singe gene expression heat maps for the tissue specificity analyses in the general population

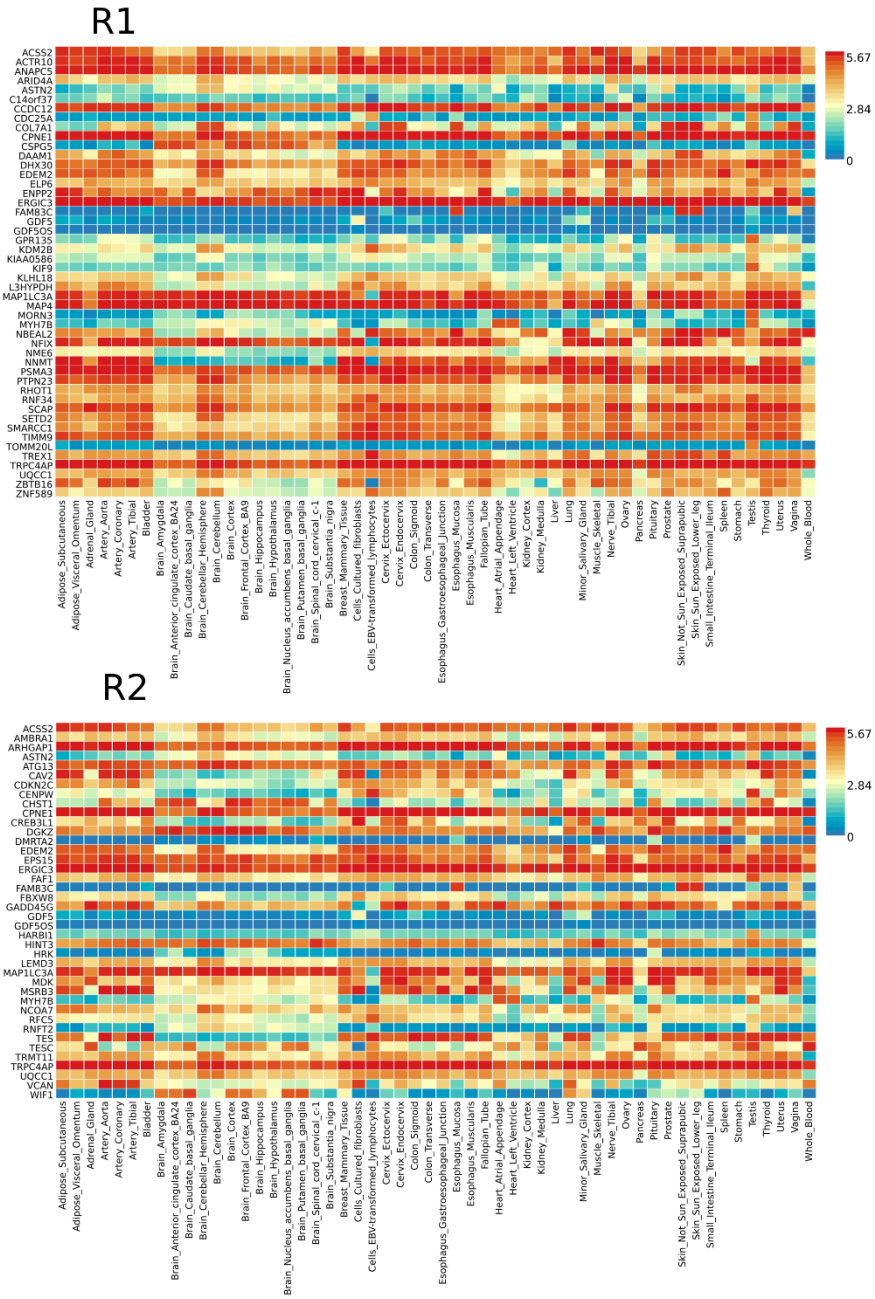

The gene-level heatmap displays the average expression per label (log_2 transformed) using data from GTEx v8 54 tissue types (above) and 30 general tissue types (below). Genes and tissue/organs are ordered in alphabetical order.

eFigure 7: The longitudinal rate of change of R1 and R2 neuroanatomical dimensions of brain atrophy in the MCI/AD population.

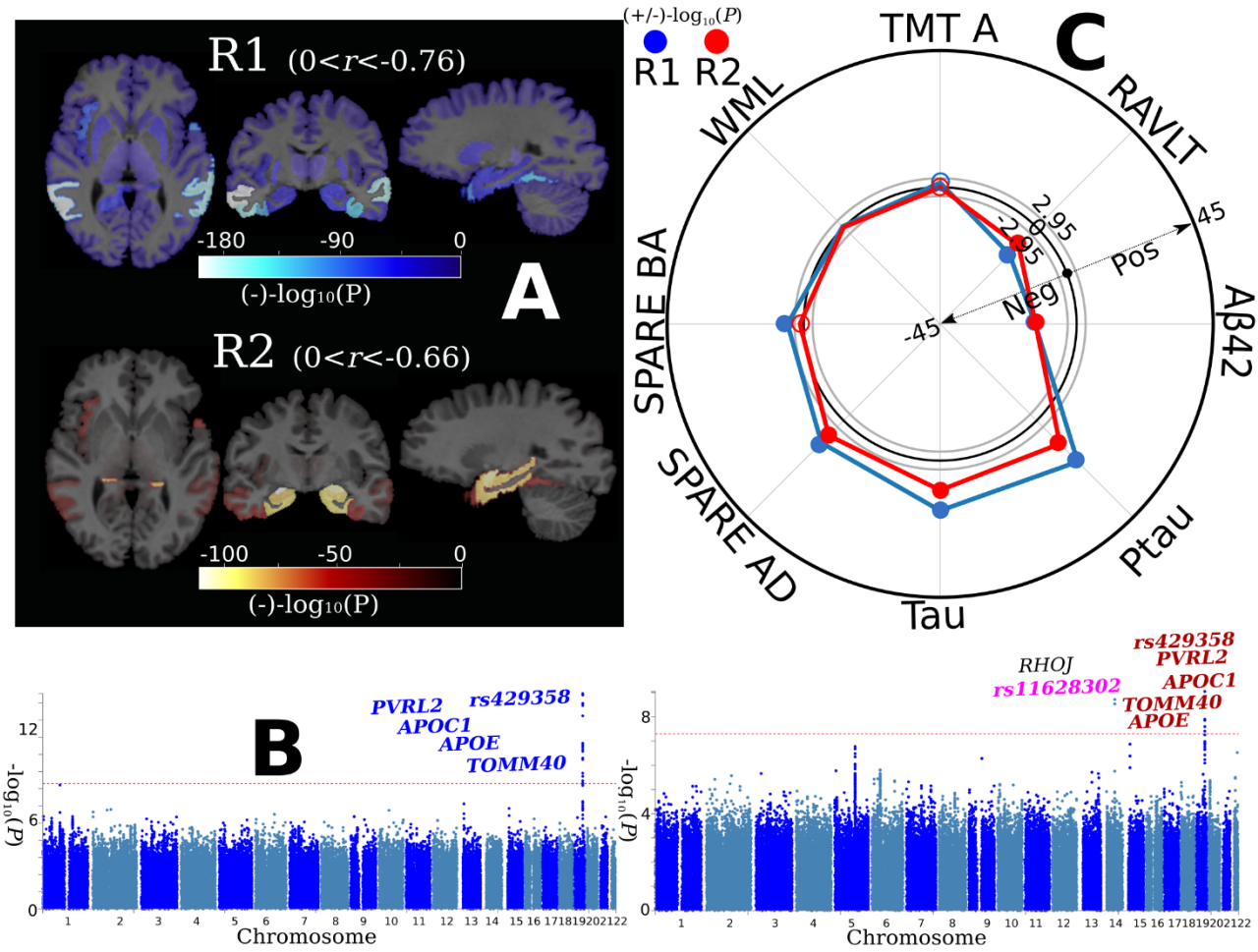

A) Longitudinal brain association studies show that the R1 dimension exhibits widespread brain atrophy, whereas the R2 dimension displays focal medial temporal lobe atrophy. We first derived the rate of change of the 119 GM ROIs and the R1 and R2 dimensions using a linear mixed effect model; a linear regression model was then fit to the rate of change of the ROIs, R1, and R2 to derive the beta value of each ROI. A negative value denotes longitudinal brain atrophy with a negative coefficient of the rate of change in the linear regression model. The range of *r* for each dimension is also shown. Of note, the sample size (*N*) for R1 and R2 is the same for each ROI. **B)** Genome-wide association studies demonstrate that the R1 and R2 dimensions are both associated with variants related to *APOE* genes (genome-wide P-value threshold with the red line: $-\log_{10}$(P-value) > 7.30). We associated each common variant with R1 and R2 using the whole-genome sequencing data from ADNI. Gene annotations were performed via positional, expression quantitative trait loci, and chromatin interaction mappings using FUMA.[44] We then manually queried whether they were previously associated with AD-related traits in the GWAS Catalog.[43] Blue and Red-colored loci/genes indicate variants associated with AD-related traits in previous literature for R1 and R2, respectively. **C)** Clinical association studies show that the R1 and R2 dimensions are associated with SPARE-AD[37], the CSF level of tau, ptau, and amyloid.

eFigure 8: Distributions of the R1 and R2 dimensions of Surreal-GAN and the P1, P2, P3, and P4 dimensions of Smile-GAN

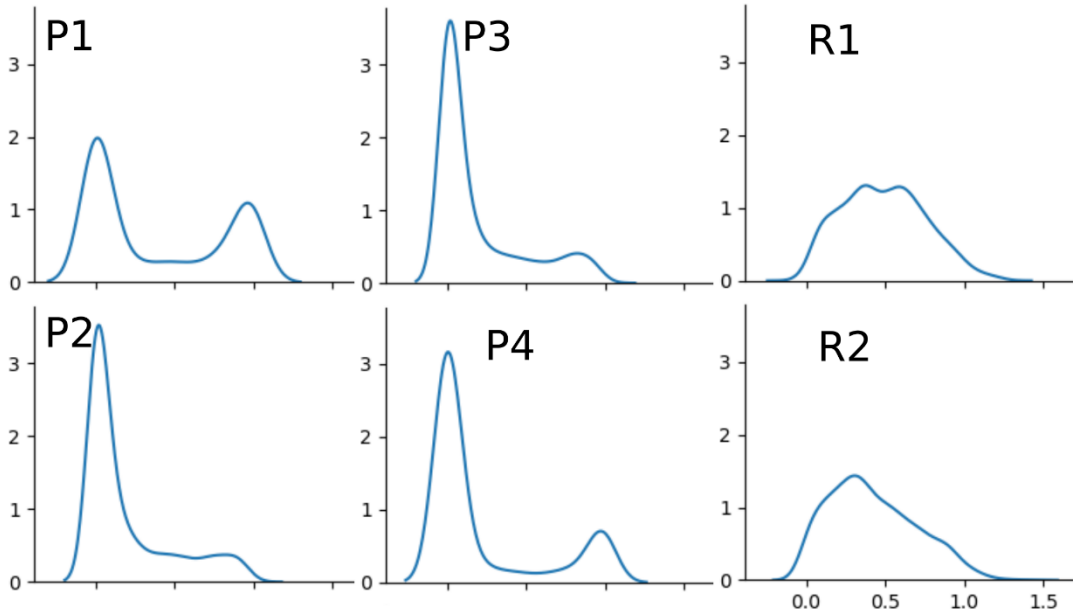

By modeling, Surreal-GAN's R1 and R2 dimensions are more appropriate and statistically powerful for continuous trait-based GWAS analyses as continuous dimensional scores. In contrast, the four subtype probability scores of Smile-GAN are better instruments for case-control GWAS as categorical variables. We used ADNI data to show that the R1 and R2 dimension scores were approximately normally distributed, and the P1, P2, P3, and P4 dimension scores followed bimodal distributions. Of note, we performed an inverse-normal transformation[12] to enable the phenotype/trait of interest to be normally distributed.

eFigure 9: Best-fit model of the PRS calculation in the MCI/AD population

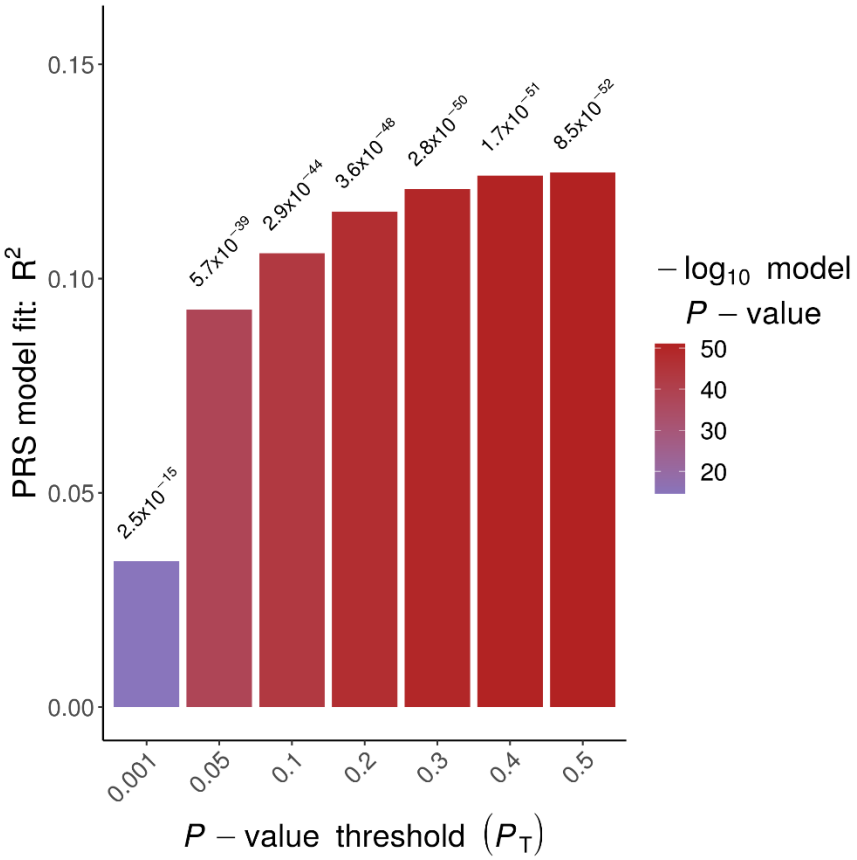

We adopted a classic clumping + thresholding (C+T) approach[13] to calculate the PRS of AD for all participants from ADNI and UKBB (**Method 6E**). To approximate the "best-fit" PRS, we performed a logistic regression using the PRS calculated at different P-value thresholds (0.001, 0.05, 0.1, 0.2, 0.3, 0.4, and 0.5), controlling for age, sex, and the first five genetic PCs. We chose the P-value threshold (0.5) based on the PRS that explains the highest phenotypic variance (R^2) (AD vs. CU in ADNI).

eTable 1: Brain association studies for the MCI/AD population from ADNI and BLSA.

Each ROI was fit with a linear regression model by controlling covariates. $-\log_{10}$(P-value) and Pearson's correlation (*r*) are reported. For the P-values, we also added the sign of the ROI's beta coefficient values to indicate the effect's direction. The threshold for Bonferroni corrected $-\log_{10}$(P-value) is > 3.38. For the *r* values, the ROIs that did not survive the multiple comparisons or showed a positive *r* (negative *r* means brain atrophy) are assigned a value of 0 for visualization purposes.

ROI	R1: sign[$-\log_{10}$(P-value)]	R2: sign[$-\log_{10}$(P-value)]	R1: *r*	R2: *r*
Right Accumbens Area	-7.50571	-18.5683	-0.13385	-0.22157
Left Accumbens Area	-4.57493	-16.6058	-0.10096	-0.21176
Right Amygdala	-12.1396	-281.515	-0.17085	-0.65027
Left Amygdala	-13.421	-262.174	-0.17854	-0.63577
Right Caudate	4.47843	0.06662	0.03963	0
Left Caudate	3.80988	0.01493	0.0358	0
Right Cerebellum Exterior	-1.42046	-1.43982	0	0
Left Cerebellum Exterior	-0.89444	-1.43875	0	0
Right Hippocampus	-7.10095	-273.254	-0.12845	-0.65086
Left Hippocampus	-4.85907	-286.073	-0.10114	-0.66999
Right Pallidum	0.45787	-0.44775	0	0
Left Pallidum	0.90213	-0.62152	0	0
Right Putamen	-1.32989	-1.3305	0	0
Left Putamen	-1.08232	-0.87145	0	0
Right Thalamus Proper	-5.56006	-14.8387	-0.1137	-0.16236
Left Thalamus Proper	-4.7225	-11.6842	-0.10534	-0.14483
Cerebellar Vermal Lobules I-V	-2.35113	-0.08627	0	0
Cerebellar Vermal Lobules VI-VII	1.2309	0.19721	0	0
Cerebellar Vermal Lobules VIII-X	1.01513	-1.28001	0	0
Left Basal Forebrain	-3.13748	-31.1551	0	-0.30623
Right Basal Forebrain	-0.07585	-18.4305	0	-0.24177
Right ACgG anterior cingulate gyrus	-2.78765	-5.35387	0	-0.12467
Left ACgG anterior cingulate gyrus	-8.48968	-2.56191	-0.15256	0
Right AIns anterior insula	-26.1772	-16.5433	-0.23749	-0.18867
Left AIns anterior insula	-29.959	-21.3573	-0.25152	-0.21728
Right AOrG anterior orbital gyrus	-4.39974	0.14837	-0.12046	0
Left AOrG anterior orbital gyrus	-4.6851	-0.18991	-0.1193	0
Right AnG angular gyrus	-93.8132	-0.65332	-0.46814	0
Left AnG angular gyrus	-72.644	-1.2325	-0.42036	0
Right Calc calcarine cortex	0.13368	0.53457	0	0
Left Calc calcarine cortex	0.14284	1.57312	0	0
Right CO central operculum	-40.5874	-0.15535	-0.28393	0
Left CO central operculum	-53.6712	-0.88026	-0.32856	0
Right Cun cuneus	-2.36823	-0.23906	0	0
Left Cun cuneus	-1.68046	-0.22262	0	0

Right Ent entorhinal area	-11.3956	-212.355	-0.16588	-0.57772
Left Ent entorhinal area	-14.2329	-234.601	-0.17832	-0.63567
Right FO frontal operculum	-25.7413	-0.60814	-0.24631	0
Left FO frontal operculum	-21.6485	-1.82348	-0.21898	0
Right FRP frontal pole	-3.30212	1.53437	0	0
Left FRP frontal pole	-8.63073	-0.61843	-0.16264	0
Right FuG fusiform gyrus	-47.9404	-26.9014	-0.30709	-0.21163
Left FuG fusiform gyrus	-50.7759	-26.4785	-0.31803	-0.22676
Right GRe gyrus rectus	-2.45628	-3.16739	0	0
Left GRe gyrus rectus	0.0541	-2.01584	0	0
Right IOG inferior occipital gyrus	-22.9084	0.04341	-0.24389	0
Left IOG inferior occipital gyrus	-28.3487	0.1735	-0.26282	0
Right ITG inferior temporal gyrus	-128.732	-18.3864	-0.46735	-0.16197
Left ITG inferior temporal gyrus	-120.071	-20.2061	-0.46359	-0.17083
Right LiG lingual gyrus	-6.49459	-1.78258	-0.14713	0
Left LiG lingual gyrus	-2.5011	-0.47708	0	0
Right LOrG lateral orbital gyrus	0.47646	3.80038	0	0.08938
Left LOrG lateral orbital gyrus	-0.16276	0.35955	0	0
Right MCgG middle cingulate gyrus	-4.18551	-0.6196	-0.12514	0
Left MCgG middle cingulate gyrus	-3.06066	-0.00227	0	0
Right MFC medial frontal cortex	-4.06739	-6.21943	-0.0963	-0.1428
Left MFC medial frontal cortex	-0.70819	-2.32881	0	0
Right MFG middle frontal gyrus	-23.0666	6.25053	-0.23259	0.09546
Left MFG middle frontal gyrus	-28.2634	4.22507	-0.25529	0.07449
Right MOG middle occipital gyrus	-29.2134	-0.6177	-0.2844	0
Left MOG middle occipital gyrus	-36.8055	-1.00391	-0.31201	0
Right MOrG medial orbital gyrus	-6.72452	-0.67406	-0.15059	0
Left MOrG medial orbital gyrus	-0.78826	0.0603	0	0
Right MPoG postcentral gyrus medial segment	-0.22712	1.52575	0	0
Left MPoG postcentral gyrus medial segment	0.07641	1.87733	0	0
Right MPrG precentral gyrus medial segment	-0.12598	1.43652	0	0
Left MPrG precentral gyrus medial segment	-0.70782	4.12148	0	0.08423
Right MSFG superior frontal gyrus medial segment	-11.9297	0.46343	-0.17345	0
Left MSFG superior frontal gyrus medial segment	-13.114	-0.31839	-0.17525	0
Right MTG middle temporal gyrus	-155.837	-15.2718	-0.51863	-0.16543
Left MTG middle temporal gyrus	-149.597	-15.5284	-0.5215	-0.17027

Right OCP occipital pole	4.31229	0.64664	0.036	0
Left OCP occipital pole	0.93506	0.10407	0	0
Right OFuG occipital fusiform gyrus	-8.06137	0.24056	-0.15547	0
Left OFuG occipital fusiform gyrus	-27.0683	-3.09207	-0.2645	0
Right OpIFG opercular part of the inferior frontal gyrus	-17.399	-0.07107	-0.20488	0
Left OpIFG opercular part of the inferior frontal gyrus	-30.847	0.40158	-0.26572	0
Right OrIFG orbital part of the inferior frontal gyrus	-5.11808	1.5731	-0.11731	0
Left OrIFG orbital part of the inferior frontal gyrus	-3.7895	2.03442	-0.09809	0
Right PCgG posterior cingulate gyrus	-32.6246	-2.30486	-0.28065	0
Left PCgG posterior cingulate gyrus	-37.6512	-4.94491	-0.29181	-0.07176
Right PCu precuneus	-62.8395	0.22134	-0.36339	0
Left PCu precuneus	-47.6593	-0.36123	-0.32947	0
Right PHG parahippocampal gyrus	-19.1909	-189.939	-0.20697	-0.5469
Left PHG parahippocampal gyrus	-19.7229	-208.439	-0.20401	-0.57164
Right PIns posterior insula	-49.5689	-9.65035	-0.3065	-0.15683
Left PIns posterior insula	-60.8608	-6.47558	-0.33883	-0.14154
Right PO parietal operculum	-18.1403	0.86838	-0.2199	0
Left PO parietal operculum	-21.4814	0.2996	-0.23754	0
Right PoG postcentral gyrus	-16.0393	2.99274	-0.2013	0
Left PoG postcentral gyrus	-16.6346	2.15175	-0.20579	0
Right POrG posterior orbital gyrus	-0.91914	-2.81108	0	0
Left POrG posterior orbital gyrus	-0.14594	-2.28165	0	0
Right PP planum polare	-29.4866	-8.91216	-0.24271	-0.15817
Left PP planum polare	-16.8675	-7.19882	-0.18734	-0.15264
Right PrG precentral gyrus	-12.9721	9.52306	-0.17726	0.1078
Left PrG precentral gyrus	-15.5279	5.81795	-0.19317	0.08159
Right PT planum temporale	-23.4547	-0.65338	-0.23324	0
Left PT planum temporale	-28.7539	-0.77124	-0.26384	0
Right SCA subcallosal area	-0.05839	-3.30599	0	0
Left SCA subcallosal area	-0.04662	-1.18346	0	0
Right SFG superior frontal gyrus	-20.3875	1.36576	-0.22634	0
Left SFG superior frontal gyrus	-21.7389	1.42391	-0.23471	0
Right SMC supplementary motor cortex	-3.43682	-0.00728	-0.09812	0
Left SMC supplementary motor cortex	-1.81719	-0.50428	0	0

Right SMG supramarginal gyrus	-89.0207	-0.09531	-0.45635	0
Left SMG supramarginal gyrus	-93.6886	1.18687	-0.47475	0
Right SOG superior occipital gyrus	-13.1905	0.37282	-0.18002	0
Left SOG superior occipital gyrus	-7.89322	0.20519	-0.13827	0
Right SPL superior parietal lobule	-35.647	0.72415	-0.29015	0
Left SPL superior parietal lobule	-36.7243	1.40962	-0.2972	0
Right STG superior temporal gyrus	-50.1012	-4.34522	-0.33617	-0.10192
Left STG superior temporal gyrus	-58.679	-6.32759	-0.36681	-0.12603
Right TMP temporal pole	-42.0432	-87.8416	-0.30518	-0.40385
Left TMP temporal pole	-44.3756	-74.3941	-0.31169	-0.38748
Right TrIFG triangular part of the inferior frontal gyrus	-0.63125	-0.26408	0	0
Left TrIFG triangular part of the inferior frontal gyrus	-4.62617	0.29648	-0.11686	0
Right TTG transverse temporal gyrus	-1.92176	-0.36857	0	0
Left TTG transverse temporal gyrus	-4.67912	-0.00132	-0.11116	0

309

eTable 2: Identified genomic loci and mapped genes for baseline GWAS in the MCI/AD population

Locus (lead SNP)	$-\log_{10}$(P-value)	Chromosome	Mapped genes
rs429358	10.98	19	*APOE, PVRL2, APOC1, TOMM40*

eTable 3: Clinical association studies for the MCI/AD population from ADNI and BLSA. Each clinical variable/biomarker was fit with a linear regression model by controlling covariates. $-\log_{10}$(P-value) and the coefficient of each variable/biomarker (beta) are reported. For the P-values, we added the sign of the variable's beta coefficient values to indicate the effect's direction. The threshold for Bonferroni corrected $-\log_{10}$(P-value) is > 2.95. For the beta values, the ROIs that did not survive the multiple comparisons are assigned a value of 0.

Variable	R1: sign[$-\log_{10}$(P-value)]	R2: sign[$-\log_{10}$(P-value)]	R1: beta	R2: beta
FAQ_Total	27.553	28.8057	0.0115	0.01237
CDR_Global	19.4197	14.7913	0.3215	0.29347
CDR_SOB	25.1713	25.8645	0.04496	0.04693
NPIQ_Total	1.98106	0.82936	0	0
DSST	-9.43994	-0.04787	-0.00837	0
TMT_A	41.8293	0.27449	0.00347	0
TMT_B	43.8428	2.95569	0.00122	0.00032
MMSE	-27.793	-29.9245	-0.03047	-0.03249
Digit_Span_Backward	-5.19651	-0.29222	-0.02402	0
Digit_Span_Forward	-1.232	-0.87773	0	0
MOCA	-19.1169	-12.0298	-0.02151	-0.01697
BNT	-14.9887	-16.0565	-0.01339	-0.01414
RAVLT	-24.1567	-38.206	-0.00431	-0.00567
RAVLT_IM	-27.8745	-30.1843	-0.00725	-0.00792
RAVLT_Short	-13.0604	-38.1494	-0.01483	-0.02665
RAVLT_Long	-13.2972	-37.6006	-0.01412	-0.02501
LM_DEL_A	-21.6429	-60.621	-0.01749	-0.03036
LM_IM_A	-28.0603	-31.5233	-0.01911	-0.0213
ANI_Fluency	-27.8458	-10.4616	-0.01424	-0.00907
VEG_Fluency	-12.1705	-4.17084	-0.02157	-0.01279
TS_RATIO	0.08455	0.82137	0	0
TS_RATIO_ADJ	0.09716	0.64491	0	0
BNT_percent	-14.9887	-16.0565	-0.00402	-0.00424
Cholesterol	0.10488	0.30897	0	0
Diastole	0.53221	-0.23115	0	0
Glucose	0.02649	-0.56589	0	0
Systole	4.03676	-0.40777	0.00155	0
Triglycerides	-0.70672	0.10056	0	0
ABETA42_ADNI	-16.6712	-9.64753	-0.00018	-0.00014
PTAU	5.69056	6.12353	0.00286	0.00299
TAU	4.7303	7.25391	0.00029	0.00036
Diabetes	-0.00052	1.41286	0	0
Hypertension	2.00269	0.027	0	0
Diagnosis_Depression	-0.44864	0.047	0	0
Alcoholic	0.89498	0.32819	0	0
Family_History_Dementia	-1.84702	-0.25455	0	0
Ethnicity	0.80007	0.04149	0	0
Height	-0.57955	0.70593	0	0
BMI	-0.97997	-7.32202	0	-0.00838
Weight	-1.57751	-5.66086	0	-0.0026
SPARE_AD	109.59	201.144	0.11401	0.1527
SPARE_BA	54.6991	8.33545	0.0116	0.00471
AV45_PET_ADNI	8.33865	4.19236	0.20317	0.13769
FDG	-52.5638	-10.3312	-0.82696	-0.37305
WMLS_Volume_701	6.1794	1.29141	0.02575	0

eTable 4: Brain association studies for the general population from UKBB. Each ROI was fit with a linear regression model by controlling covariates. $-\log_{10}$(P-value) and Pearson's correlation (*r*) are reported. For the P-values, we also added the sign of the ROI's beta coefficient values to indicate the effect's direction. The threshold for Bonferroni corrected $-\log_{10}$(P-value) is > 3.38. For the *r* values, the ROIs that did not survive the multiple comparisons or showed a positive *r* (negative *r* means brain atrophy) are assigned a value of 0 for visualization purposes.

ROI	R1: sign[$-\log_{10}$(P-value)]	R2: sign[$-\log_{10}$(P-value)]	R1: *r*	R2: *r*
Right Accumbens Area	1.41659	-182.266	0	-0.0492
Left Accumbens Area	1.61428	-167.936	0	-0.03835
Right Amygdala	-98.726	-330	-0.15118	-0.33719
Left Amygdala	-56.4488	-330	-0.12555	-0.31386
Right Caudate	300	-44.3821	0.11226	-0.02326
Left Caudate	300	-37.3245	0.10616	-0.00926
Right Cerebellum Exterior	-9.33216	-151.136	-0.08723	0.00104
Left Cerebellum Exterior	-12.3741	-116.615	-0.09151	0.0084
Right Hippocampus	0.12934	-330	0	-0.36498
Left Hippocampus	1.61488	-330	0	-0.34206
Right Pallidum	22.3496	-27.02	-0.038	0.0343
Left Pallidum	21.293	-47.475	-0.02817	0.01584
Right Putamen	-0.82029	-69.6543	0	0.00366
Left Putamen	-0.3018	-59.1727	0	0.00934
Right Thalamus Proper	-28.9526	-87.2289	-0.12938	0.04023
Left Thalamus Proper	-33.4427	-92.0801	-0.13339	0.04002
Cerebellar Vermal Lobules I-V	-29.5876	-7.76566	-0.10368	0.03997
Cerebellar Vermal Lobules VI-VII	0.80143	-21.3033	0	-0.00421
Cerebellar Vermal Lobules VIII-X	-3.851	-87.7558	-0.05945	-0.02211
Left Basal Forebrain	137.211	-64.3165	0.06201	-0.03614
Right Basal Forebrain	104.834	-110.189	0.04623	-0.05927
Right ACgG anterior cingulate gyrus	-0.21265	-5.72052	0	0.03231
Left ACgG anterior cingulate gyrus	-10.4907	-5.89634	-0.1117	0.04079
Right AIns anterior insula	-90.4988	-112.325	-0.15479	-0.00513
Left AIns anterior insula	-87.4626	-84.7404	-0.15327	0.00519
Right AOrG anterior orbital gyrus	-3.62996	142.979	-0.08145	0.17176
Left AOrG anterior orbital gyrus	-5.75963	70.2007	-0.06233	0.13786
Right AnG angular gyrus	-300	13.7095	-0.37557	0.10415
Left AnG angular gyrus	-300	32.058	-0.3504	0.11536
Right Calc calcarine cortex	14.0495	84.0712	-0.02481	0.14709
Left Calc calcarine cortex	22.6608	92.9419	-0.00831	0.14631
Right CO central operculum	-300	66.8329	-0.25532	0.14862
Left CO central operculum	-300	15.5315	-0.28549	0.11619
Right Cun cuneus	-1.40722	25.3579	0	0.11906
Left Cun cuneus	0.01067	35.5432	0	0.12482
Right Ent entorhinal area	-15.7387	-330	-0.07315	-0.33158
Left Ent entorhinal area	-37.3154	-330	-0.09629	-0.38061

Right FO frontal operculum	-283.5	2.60188	-0.20745	0
Left FO frontal operculum	-174.006	67.8112	-0.18019	0.14426
Right FRP frontal pole	-12.934	178.43	-0.11962	0.1829
Left FRP frontal pole	-43.9357	73.5255	-0.13305	0.1402
Right FuG fusiform gyrus	-198.547	-36.8795	-0.17519	0.03427
Left FuG fusiform gyrus	-300	-18.9938	-0.21721	0.04813
Right GRe gyrus rectus	-3.66473	9.10609	-0.08331	0.09133
Left GRe gyrus rectus	0.7205	15.698	0	0.09976
Right IOG inferior occipital gyrus	-15.7166	5.87919	-0.10042	0.08228
Left IOG inferior occipital gyrus	-7.20403	113.876	-0.10013	0.14714
Right ITG inferior temporal gyrus	-300	0.85369	-0.32453	0
Left ITG inferior temporal gyrus	-300	15.0401	-0.3341	0.104
Right LiG lingual gyrus	-53.927	-20.8439	-0.13147	0.04954
Left LiG lingual gyrus	-6.76542	26.077	-0.10231	0.11848
Right LOrG lateral orbital gyrus	18.2409	132.453	-0.0165	0.1532
Left LOrG lateral orbital gyrus	36.4951	210.898	-0.00863	0.19322
Right MCgG middle cingulate gyrus	-3.90798	25.1491	-0.09126	0.10476
Left MCgG middle cingulate gyrus	-8.4155	15.4716	-0.0963	0.09492
Right MFC medial frontal cortex	1.78702	-3.97811	0	0.04703
Left MFC medial frontal cortex	21.2943	2.90145	-0.02022	0
Right MFG middle frontal gyrus	-129.233	279.61	-0.17922	0.21173
Left MFG middle frontal gyrus	-109.494	330	-0.17173	0.22885
Right MOG middle occipital gyrus	-149.532	88.1747	-0.1873	0.14692
Left MOG middle occipital gyrus	-300	18.7585	-0.26727	0.10437
Right MOrG medial orbital gyrus	15.4308	9.37965	-0.06111	0.09879
Left MOrG medial orbital gyrus	106.518	15.6631	0.00145	0.0948
Right MPoG postcentral gyrus medial segment	18.4511	106.131	-0.00525	0.14145
Left MPoG postcentral gyrus medial segment	0.94506	79.6395	0	0.13066
Right MPrG precentral gyrus medial segment	18.3772	193.817	-0.01673	0.19332
Left MPrG precentral gyrus medial segment	69.2107	147.742	0.03316	0.16704
Right MSFG superior frontal gyrus medial segment	-76.67	244.578	-0.15288	0.20867
Left MSFG superior frontal gyrus medial segment	-91.3879	168.41	-0.15268	0.19107
Right MTG middle temporal gyrus	-300	-20.9451	-0.37466	0.05852
Left MTG middle temporal gyrus	-300	-21.69	-0.39366	0.0523
Right OCP occipital pole	197.625	84.9317	0.0602	0.13398
Left OCP occipital pole	255.843	211.639	0.06741	0.1804

Right OFuG occipital fusiform gyrus	-12.0126	94.2742	-0.0894	0.14724
Left OFuG occipital fusiform gyrus	-101.671	-3.81391	-0.14763	0.05335
Right OpIFG opercular part of the inferior frontal gyrus	-273.101	91.9958	-0.20386	0.15424
Left OpIFG opercular part of the inferior frontal gyrus	-243.767	180.399	-0.20055	0.19079
Right OrIFG orbital part of the inferior frontal gyrus	-2.27412	22.8358	0	0.09156
Left OrIFG orbital part of the inferior frontal gyrus	-0.24746	58.0824	0	0.12043
Right PCgG posterior cingulate gyrus	-209.592	-11.9412	-0.19378	0.0483
Left PCgG posterior cingulate gyrus	-262.46	-34.3738	-0.20553	0.03161
Right PCu precuneus	-300	54.9645	-0.29166	0.14355
Left PCu precuneus	-300	40.902	-0.27177	0.13637
Right PHG parahippocampal gyrus	-173.097	-330	-0.16496	-0.34984
Left PHG parahippocampal gyrus	-198.601	-330	-0.17802	-0.37505
Right PIns posterior insula	-266.472	-23.7998	-0.21771	0.04153
Left PIns posterior insula	-300	-89.6578	-0.23383	-0.00766
Right PO parietal operculum	-66.7351	66.8369	-0.14711	0.13074
Left PO parietal operculum	-102.229	85.3908	-0.1649	0.15125
Right PoG postcentral gyrus	-282.817	120.309	-0.2271	0.16294
Left PoG postcentral gyrus	-270.006	78.0722	-0.22169	0.14354
Right POrG posterior orbital gyrus	78.6402	1.4835	0.00852	0
Left POrG posterior orbital gyrus	45.1416	1.80514	-0.00667	0
Right PP planum polare	-71.6443	-43.1669	-0.14793	0.00847
Left PP planum polare	-34.4771	-11.488	-0.12538	0.03474
Right PrG precentral gyrus	-46.192	330	-0.13865	0.2993
Left PrG precentral gyrus	-45.3155	330	-0.13484	0.28293
Right PT planum temporale	-120.698	115.443	-0.16067	0.16964
Left PT planum temporale	-273.535	9.16214	-0.20004	0.10329
Right SCA subcallosal area	65.4707	-8.55722	-0.00285	0.02647
Left SCA subcallosal area	71.5098	-12.2986	0.00515	0.0165
Right SFG superior frontal gyrus	-36.5317	274.089	-0.13275	0.21365
Left SFG superior frontal gyrus	-53.0535	189.783	-0.13843	0.19185
Right SMC supplementary motor cortex	-0.03372	9.90833	0	0.09648
Left SMC supplementary motor cortex	2.78577	46.7257	0	0.13199
Right SMG supramarginal gyrus	-300	48.1282	-0.3503	0.12322

Left SMG supramarginal gyrus	-300	27.7533	-0.39415	0.11116
Right SOG superior occipital gyrus	-47.779	51.9886	-0.1022	0.12563
Left SOG superior occipital gyrus	-20.1313	186.27	-0.08898	0.18213
Right SPL superior parietal lobule	-283.018	19.7144	-0.21697	0.10935
Left SPL superior parietal lobule	-228.822	42.5037	-0.20604	0.12639
Right STG superior temporal gyrus	-285.959	59.4549	-0.22136	0.14333
Left STG superior temporal gyrus	-232.898	45.5607	-0.20047	0.13356
Right TMP temporal pole	-300	-330	-0.2528	-0.08413
Left TMP temporal pole	-300	-263.576	-0.24616	-0.05492
Right TrIFG triangular part of the inferior frontal gyrus	6.09269	7.36744	-0.02755	0.08494
Left TrIFG triangular part of the inferior frontal gyrus	0.42304	21.9329	0	0.10336
Right TTG transverse temporal gyrus	-5.83701	11.5266	-0.08222	0.09567
Left TTG transverse temporal gyrus	0.38757	1.90911	0	0

327

eTable 5: Clinical association studies for the general population from UKBB. Each clinical variable/biomarker was fit with a linear regression model by controlling covariates. $-\log_{10}$(P-value) and the coefficient of each variable/biomarker (beta) are reported. For the P-values, we added the sign of the variable's beta coefficient values to indicate the effect's direction. The threshold for Bonferroni corrected $-\log_{10}$(P-value) is > 3.08. For the beta values, the ROIs that did not survive the multiple comparisons are assigned a value of 0.

Variable	R1: sign[$-\log_{10}$(P-value)]	R2: sign[$-\log_{10}$(P-value)]	R1: beta	R2: beta
Cholesterol	-1.24939	-0.38153	0	0
Lipoprotein A	-0.53029	0.04826	0	0
HDL cholesterol	-3.9835	-1.84715	-0.01293	0
Triglycerides	13.1313	0.0063	0.00866	0
Apolipoprotein A	-0.80123	-1.81085	0	0
Apolipoprotein B	-0.20008	0.1776	0	0
C-reactive protein	3.58939	0.14067	0.0011	0
LDL direct	-1.6734	-0.00117	0	0
Glucose	7.08853	-0.86482	0.00632	0
Glycated haemoglobin (HbA1c)	14.2612	-1.67051	0.00169	0
Maternal smoking	0.78205	-0.77154	0	0
Household income	0.07764	2.15911	0	0
Education	3.18428	2.89039	0.00211	0
Ethnicity	0.63381	0.29638	0	0
Townsend Deprivation Index tertiles	2.92812	1.18548	0	0
Sleep duration	0.70548	0.29459	0	0
Easy to get up in the morning	-1.88294	3.93415	0	0.00199
Morning or evening person	1.17031	-1.66819	0	0
Nap during the day	0.66029	-0.6407	0	0
Insomnia	-0.05737	-2.81902	0	0
Snoring	0.05859	-0.11376	0	0
Daytime dozing sleeping	-0.5191	0.15494	0	0
Sleep too much	2.24252	0.2305	0	0
Sleep trouble start	-0.14304	-0.0328	0	0
Sleep trouble end	-2.39029	-0.09417	0	0
Sleep any problem	0.55325	-0.31399	0	0
Ever smoked	-0.18363	-0.28497	0	0
Smoking status	0.74339	-0.20541	0	0
Current tobacco smoking	2.64765	0.10738	0	0
Past tobacco smoking	1.72746	-0.26343	0	0

Light smokers at least 100 smokes in lifetime	-0.66022	1.70368	0	0
Age started smoking in former smokers	-1.40981	0.05561	0	0
Age stopped smoking	9.72342	-0.73592	0.00116	0
Smoking smokers in household	0.30144	0.29766	0	0
Exposure to tobacco smoke at home	0.20145	-0.10873	0	0
Exposure to tobacco smoke outside home	-0.09736	0.22288	0	0
Coffee intake	-0.60155	-2.47628	0	0
Ever vascular heart problem diagnosed	-5.01173	-0.09841	-0.01375	0
Age high blood pressure diagnosed	-1.32468	-0.7335	0	0
Diabetes diagnosed by doctor	21.3642	-2.04208	0.02258	0
Diastolic blood pressure (automated reading)	10.5304	1.43241	0.00074	0
Pulse rate (automated reading)	1.26898	0.13024	0	0
Systolic blood pressure (automated reading)	1.83095	0.16135	0	0
Pair matching_1	6.51554	0.63956	0.0065	0
Pair matching_2	7.76305	1.38813	7.64E-05	0
Reaction time_1	2.32465	5.09847	0	4.21E-05
Reaction time_2	0.43728	0.68777	0	0
VNR	-17.0222	-0.78106	-0.00452	0
Prospective memory_1	1.46794	-0.65534	0	0
Prospective memory_2	2.34823	8.31264	0	0.01136
Pair_matching_2 (online)	0.9509	0.25269	0	0
Pair_matching_3 (online)	0.7003	0.92109	0	0
Symbolic digital substitution_1 (online)	-7.16303	-0.63596	-0.0017	0
Symbolic digital substitution_2 (online)	2.12657	3.19173	0	6.92E-07
VNR (online)	-7.91013	-1.46754	-0.00399	0
TMT-A	3.02215	-0.08899	0	0
TMT-B	8.47316	-2.29301	2.91E-05	0
AD_by_proxy	-2.24382	0.12213	0	0
SPARE_AD	136	250	0.12096	0.1268
SPARE_BA	236.859	-46.3563	0.00646	-0.00263
WMLS_Volume_701	120.241	2.06141	6.89E-06	0

334

eTable 6: Identified genomic loci and mapped genes for GWAS in the general population

R1:

Locus	P-value	Chromosome	Mapped genes
rs13079098	4.91E-09	3	*MAP4, PTPN23, KIF9, COL7A1, CSPG5, KLHL18, SCAP, DHX30, NBEAL2, CCDC12, ELP6, CDC25A, ZNF589,NME6, SMARCC1, SETD2,TREX1*
rs17669337	4.51E-11	5	--
rs2028849	8.76E-10	8	*ENPP2*
rs11794318	3.02E-09	9	*ASTN2*
rs3825045	1.98E-08	11	*ZBTB16, NNMT*
rs9795600	1.12E-08	12	*ANAPC5, KDM2B, MORN3, RNF34*
rs11158204, rs5809016	1.31E-15, 1.30E-15	14	*GPR135, TOMM20L, AL132989.1, C14orf37, L3HYPDH, ACTR10, TIMM9, KIAA0586, DAAM1, ARID4A, PSMA3*
rs34395183	3.70E-08	17	*RHOT1*
rs68175985	2.11E-08	19	*NFIX*
rs201662360	2.41E-09	20	*MYH7B, EDEM2, TRPC4AP, UQCC1, MAP1LC3A, GDF5, ERGIC3, FAM83C, ACSS2, GDF5OS, CPNE1*

R2:

Locus	P-value	Chromosome	Mapped genes
rs76606504	4.48E-08	1	*EPS15, CDKN2C, DMRTA2, FAF1*
rs3860446, rs10184573	3.02E-09, 2.09E-08	2	--
rs309587	4.06E-09	5	*VCAN*
rs117892760	1.68E-17	6	*CENPW, HINT3, NCOA7, TRMT11*
rs55885771	1.88E-08	7	*CAV2, TES*
rs1475536, rs2416560	3.82E-13, 2.16E-08	9	*GADD45G*
rs58163343	2.10E-08	11	*MDK, AMBRA1, DGKZ,CREB3L1, ARHGAP1, ATG13, CHST1, HARBI1*
rs10774183, rs17178006, rs77956314	9.22E-20, 5.30E-29, 9.98E-29	12	*TESC, RFC5, HRK, RNFT2, WIF1, MSRB3, LEMD3, FBXW8*
rs143383	5.46E-11	20	*CPNE1, GDF5OS, ACSS2, GDF5, ERGIC3, ERGIC3, MAP1LC3A, UQCC1, TRPC4AP, EDEM2, MYH7B*

eTable 7: Gene set enrichment analysis results in the general population

R1:

Category	Gene Set	P-value	Overlapped genes
GWAS Catalog	Waist-to-hip ratio	2.23E-11	*ACSS2:MYH7B:TRPC4AP:EDEM2: FAM83C:UQCC1:GDF5:ERGIC3:CPNE1*
GWAS Catalog	Huntington's disease	5.63E-09	*CCDC12:NBEAL2:SETD2:KIF9:KLHL18*
GWAS Catalog	Prothrombin time	8.07E-07	*MYH7B:TRPC4AP:EDEM2*
GWAS Catalog	QRS	4.87E-05	*MYH7B:EDEM2*
GWAS Catalog	Spine bone	7.82E-05	*UQCC1:GDF5*
GWAS Catalog	Height	1.79E-04	*FAM83C:UQCC1:GDF5OS:GDF5:ERGIC3: CPNE1:ENPP2*
GWAS Catalog	Blood protein	1.99E-04	*MYH7B:TRPC4AP:EDEM2:UQCC1:GDF5OS: GDF5:CPNE1:CDC25A:ZNF589:COL7A1*
Chemical and Genetic perturbation	NIKOLSKY BREAST CANCER 20Q11 AMPLICON	2.84E-22	*MAP1LC3A:ACSS2:MYH7B:TRPC4AP: EDEM2:FAM83C:UQCC1:GDF5:ERGIC3:CPNE1*
Chemical and Genetic perturbation	LASTOWSKA NEUROBLASTOMA COPY NUMBER DN	9.36E-07	*CCDC12:SETD2:SCAP:ELP6:SMARCC1: DHX30:CDC25A:ZNF589:NME6*
Chemical and Genetic perturbation	PURBEY TARGETS OF CTBP1 AND SATB1 UP	3.54E-06	*ARID4A:GPR135:CPNE1:COL7A1*
Chemical and Genetic perturbation	STREICHER LSM1 TARGETS UP	3.05E-05	*ARID4A:DAAM1:CDC25A*
Immunologic signatures	GSE25123 CTRL VS IL4 AND ROSIGLITAZONE STIM PPARG KO MACROPHAGE DN	7.17E-06	*ZBTB16:ANAPC5:NFIX:ACSS2:KLHL18*
Curated gene sets	NIKOLSKY BREAST CANCER 20Q11 AMPLICON	2.84E-22	*MAP1LC3A:ACSS2:MYH7B:TRPC4AP:EDEM2: FAM83C:UQCC1:GDF5:ERGIC3:CPNE1*
Curated gene sets	LASTOWSKA NEUROBLASTOMA COPY NUMBER DN	9.36E-07	*CCDC12:SETD2:SCAP:ELP6:SMARCC1: DHX30:CDC25A:ZNF589:NME6*
Curated gene sets	PURBEY TARGETS OF CTBP1 AND SATB1 UP	3.53E-06	*ARID4A:GPR135:CPNE1:COL7A1*
Curated gene sets	REACTOME CHROMATIN ORGANIZATION	2.93E-05	*KDM2B:ARID4A:SETD2:ELP6:SMARCC1*
Curated gene sets	STREICHER LSM1 TARGETS UP	3.05E-05	*ARID4A:DAAM1:CDC25A*
Reactome	REACTOME CHROMATIN ORGANIZATION	2.93E-05	*KDM2B:ARID4A:SETD2:ELP6:SMARCC1*

R2:

Category	Gene Set	P-value	Overlapped genes
GWAS Catalog	Hippocampus	2.19E-22	*WIF1:LEMD3:MSRB3:RNFT2:HRK:FBXW8:TESC:ASTN2*
GWAS Catalog	Dentate gyrus	2.19E-22	*WIF1:LEMD3:MSRB3:RNFT2:HRK:FBXW8:TESC:ASTN2*
GWAS Catalog	Alzheimer's disease	1.36E-13	*CREB3L1:DGKZ:MDK:AMBRA1:HARBI1:ATG13:ARHGAP1*
GWAS Catalog	Waist-to-hip ratio	4.66E-12	*ACSS2:MYH7B:TRPC4AP:EDEM2:FAM83C:UQCC1: GDF5:ERGIC3:CPNE1*
GWAS Catalog	Immunoglobulin A	2.95E-11	*DGKZ:MDK:AMBRA1:HARBI1:ATG13*
GWAS Catalog	Baldness	4.19E-07	*DMRTA2:FAF1:CDKN2C:HINT3:TRMT11:CENPW*
GWAS Catalog	Prothrombin time	4.92E-07	*MYH7B:TRPC4AP:EDEM2*
GWAS Catalog	Schizophrenia	3.59E-07	*CREB3L1:DGKZ:MDK:AMBRA1:HARBI1:ATG13:ARHGAP1:ERGIC3*
GWAS Catalog	Autism spectrum disorder	1.74E-05	*CREB3L1:DGKZ:MDK:AMBRA1:HARBI1:ATG13:ARHGAP1*
GWAS Catalog	Reaction time	2.42E-05	*DGKZ:ATG13:ARHGAP1*
GWAS Catalog	QRS	3.52E-05	*MYH7B:EDEM2*
GWAS Catalog	FEV1	4.72E-05	*FAF1:MSRB3:UQCC1:ASTN2*
GWAS Catalog	Spine bone	5.65E-05	*UQCC1:GDF5*
GWAS Catalog	Height	6.20E-05	*FAM83C:UQCC1:GDF5OS:GDF5:ERGIC3:CPNE1:CENPW*
GWAS Catalog	Ischemic stroke	1.13E-04	*FAF1:CDKN2C*
GWAS Catalog	Alzheimer's disease (onset)	1.69E-04	*RNFT2:HRK*
GWAS Catalog	Neuroticism	1.98E-04	*ARHGAP1:RFC5:CENPW*
Chemical and Genetic perturbation	NIKOLSKY BREAST CANCER 20Q11 AMPLICON	4.67E-23	*MAP1LC3A:ACSS2:MYH7B:TRPC4AP:EDEM2 :FAM83C:UQCC1:GDF5:ERGIC3:CPNE1*
Chemical and Genetic perturbation	ROVERSI GLIOMA_COPY_NUMBER_UP	9.75E-08	*CHST1:CREB3L1:DGKZ:MDK:ARHGAP1*
Chemical and Genetic perturbation	CHICAS RB1 TARGETS CONFLUENT	3.04E-06	*CREB3L1:MDK:ARHGAP1:MSRB3:GDF5:TES:CAV2*
Chemical and Genetic perturbation	WANG CLIM2 TARGETS UP	9.95E-06	*DGKZ:ATG13:UQCC1:CAV2:ASTN2*
Chemical and Genetic perturbation	HADDAD B LYMPHOCYTE PROGENITOR	1.62E-05	*CDKN2C:RNFT2:HRK:RFC5:GADD45G*
Immunologic signatures	GSE7509 UNSTIM VS TNFA IL1B IL6 PGE STIM DC UP	7.62E-05	*MAP1LC3A:TRPC4AP:EDEM2:HINT3*
Immunologic signatures	GSE17721 CTRL VS LPS 6H BMDC UP	7.92E-05	*FAF1:CDKN2C:EPS15:GADD45G*
Immunologic signatures	GSE17721 CTRL VS CPG 1H BMDC UP	7.92E-05	*CDKN2C:CREB3L1:DGKZ:GADD45G*
Immunologic signatures	GSE5960 TH1 VS ANERGIC TH1 DN	7.92E-05	*CREB3L1:MDK:TRPC4AP:TES*
Curated gene sets	NIKOLSKY BREAST CANCER 20Q11 AMPLICON	4.67E-23	*MAP1LC3A:ACSS2:MYH7B:TRPC4AP:EDEM2: FAM83C:UQCC1:GDF5:ERGIC3:CPNE1*
Curated gene sets	CHICAS RB1 TARGETS CONFLUENT	3.04E-06	*CREB3L1:MDK:ARHGAP1:MSRB3:GDF5:TES:CAV2*
Curated gene sets	WANG CLIM2 TARGETS UP	9.96E-06	*DGKZ:ATG13:UQCC1:CAV2:ASTN2*
Curated gene sets	HADDAD B LYMPHOCYTE PROGENITOR	1.62E-05	*CDKN2C:RNFT2:HRK:RFC5:GADD45G*

eTable 8: Brain association studies for the cognitively unimpaired (CU) population from ADNI and BLSA. Each ROI was fit with a linear regression model by controlling covariates. $-\log_{10}$(P-value) and Pearson's correlation (*r*) are reported. For the P-values, we also added the sign of the ROI's beta coefficient values to indicate the effect's direction. The threshold for Bonferroni corrected $-\log_{10}$(P-value) is > 3.38. For the *r* values, the ROIs that did not survive the multiple comparisons or showed a positive *r* (negative *r* means brain atrophy) are assigned a value of 0 for visualization purposes.

ROI	R1: sign[$-\log_{10}$(P-value)]	R2: sign[$-\log_{10}$(P-value)]	R1: *r*	R2: *r*
Right Accumbens Area	0.02422	-9.97664	0	-0.01843
Left Accumbens Area	-0.74491	-5.85925	0	0.02215
Right Amygdala	-2.48324	-116.367	0	-0.32023
Left Amygdala	-0.49706	-128.307	0	-0.35099
Right Caudate	13.1087	0.31537	0.11551	0
Left Caudate	13.4701	-0.09992	0.12082	0
Right Cerebellum Exterior	-1.22265	-3.19868	0	0
Left Cerebellum Exterior	-2.79468	-3.67638	0	-0.02158
Right Hippocampus	-3.06027	-170.382	0	-0.41714
Left Hippocampus	-1.10676	-155.177	0	-0.37296
Right Pallidum	0.58246	0.34191	0	0
Left Pallidum	0.24224	-0.00182	0	0
Right Putamen	-1.31769	-1.29282	0	0
Left Putamen	-0.65712	-1.74109	0	0
Right Thalamus Proper	-0.79193	-3.88437	0	0.02803
Left Thalamus Proper	-1.17706	-3.62831	0	0.03503
Cerebellar Vermal Lobules I-V	-4.13432	-0.07438	-0.08298	0
Cerebellar Vermal Lobules VI-VII	0.66074	1.69841	0	0
Cerebellar Vermal Lobules VIII-X	-0.13531	-3.29106	0	0
Left Basal Forebrain	1.52331	-4.46827	0	0.01873
Right Basal Forebrain	1.44434	-2.36463	0	0
Right ACgG anterior cingulate gyrus	-0.14346	0.11605	0	0
Left ACgG anterior cingulate gyrus	-0.47404	2.92022	0	0
Right AIns anterior insula	-6.19075	-0.90888	-0.09814	0
Left AIns anterior insula	-3.9446	-1.54477	-0.08014	0
Right AOrG anterior orbital gyrus	-0.25551	0.10997	0	0
Left AOrG anterior orbital gyrus	-0.0104	0.51573	0	0
Right AnG angular gyrus	-44.3189	2.29514	-0.25141	0
Left AnG angular gyrus	-34.0593	2.69873	-0.23458	0
Right Calc calcarine cortex	0.95427	1.3806	0	0
Left Calc calcarine cortex	1.60106	2.3469	0	0
Right CO central operculum	-21.4518	3.68169	-0.1368	0.17626
Left CO central operculum	-30.7951	2.13474	-0.21934	0
Right Cun cuneus	-1.30454	0.15463	0	0
Left Cun cuneus	-0.85633	0.089	0	0

Right Ent entorhinal area	-0.48193	-94.2836	0	-0.31755
Left Ent entorhinal area	-1.47259	-112.902	0	-0.36522
Right FO frontal operculum	-4.71612	3.50542	-0.08757	0.14387
Left FO frontal operculum	-7.80919	4.71573	-0.06409	0.18985
Right FRP frontal pole	-1.78447	7.39516	0	0.1951
Left FRP frontal pole	-6.25577	2.96574	-0.0413	0
Right FuG fusiform gyrus	-11.3483	-3.99863	-0.16477	-0.02522
Left FuG fusiform gyrus	-20.5362	-4.72936	-0.20459	-0.0245
Right GRe gyrus rectus	-0.99644	0.36732	0	0
Left GRe gyrus rectus	0.08139	-0.71079	0	0
Right IOG inferior occipital gyrus	-0.56007	0.76815	0	0
Left IOG inferior occipital gyrus	0.10238	3.30977	0	0
Right ITG inferior temporal gyrus	-79.5925	-0.43182	-0.36824	0
Left ITG inferior temporal gyrus	-54.6705	-2.45957	-0.33551	0
Right LiG lingual gyrus	-1.10594	-1.03965	0	0
Left LiG lingual gyrus	0.21369	-0.22744	0	0
Right LOrG lateral orbital gyrus	5.96812	7.65209	0.03279	0.11501
Left LOrG lateral orbital gyrus	1.44208	8.75206	0	0.19311
Right MCgG middle cingulate gyrus	0.07973	3.16878	0	0
Left MCgG middle cingulate gyrus	-0.05795	4.14204	0	0.13171
Right MFC medial frontal cortex	1.08139	-1.51896	0	0
Left MFC medial frontal cortex	3.58839	-0.78213	0.05774	0
Right MFG middle frontal gyrus	-2.90496	15.8988	0	0.18026
Left MFG middle frontal gyrus	-3.27888	15.1054	0	0.18331
Right MOG middle occipital gyrus	-13.2238	2.98902	-0.18857	0
Left MOG middle occipital gyrus	-22.4568	0.45539	-0.21777	0
Right MOrG medial orbital gyrus	2.26776	3.89384	0	0.11455
Left MOrG medial orbital gyrus	7.10968	3.86849	0.00986	0.07279
Right MPoG postcentral gyrus medial segment	4.26336	2.28323	0.08468	0
Left MPoG postcentral gyrus medial segment	-0.976	0.98263	0	0
Right MPrG precentral gyrus medial segment	1.7376	2.1092	0	0
Left MPrG precentral gyrus medial segment	3.86669	3.14416	0.03619	0
Right MSFG superior frontal gyrus medial segment	-1.9857	3.71251	0	0.15299
Left MSFG superior frontal gyrus medial segment	-3.80664	1.50272	-0.03031	0
Right MTG middle temporal gyrus	-78.7893	-1.42619	-0.32799	0
Left MTG middle temporal gyrus	-88.6047	-3.09453	-0.35737	0

Right OCP occipital pole	9.10347	1.57333	0.08553	0
Left OCP occipital pole	11.9957	7.11525	0.12456	0.1673
Right OFuG occipital fusiform gyrus	-0.44305	1.93927	0	0
Left OFuG occipital fusiform gyrus	-7.02536	-2.44769	-0.14617	0
Right OpIFG opercular part of the inferior frontal gyrus	-11.9213	4.95626	-0.13442	0.16631
Left OpIFG opercular part of the inferior frontal gyrus	-11.1503	2.94214	-0.10786	0
Right OrIFG orbital part of the inferior frontal gyrus	0.70391	2.36786	0	0
Left OrIFG orbital part of the inferior frontal gyrus	1.81898	2.94668	0	0
Right PCgG posterior cingulate gyrus	-15.3029	-1.77989	-0.19969	0
Left PCgG posterior cingulate gyrus	-11.5197	-0.61498	-0.17758	0
Right PCu precuneus	-29.9026	2.54008	-0.2271	0
Left PCu precuneus	-19.8806	1.80214	-0.17966	0
Right PHG parahippocampal gyrus	-16.582	-109.089	-0.16942	-0.32044
Left PHG parahippocampal gyrus	-11.9967	-127.379	-0.16249	-0.35343
Right PIns posterior insula	-12.4309	-0.60413	-0.14632	0
Left PIns posterior insula	-19.8889	-2.07986	-0.1697	0
Right PO parietal operculum	-1.49742	3.12846	0	0
Left PO parietal operculum	-2.05314	5.69654	0	0.14372
Right PoG postcentral gyrus	-11.147	15.9636	-0.14717	0.22742
Left PoG postcentral gyrus	-7.26167	6.01063	-0.13704	0.15154
Right POrG posterior orbital gyrus	1.78048	0.45129	0	0
Left POrG posterior orbital gyrus	3.11751	0.99777	0	0
Right PP planum polare	-10.2705	0.14541	-0.06999	0
Left PP planum polare	-2.33648	1.43902	0	0
Right PrG precentral gyrus	-1.58787	19.0602	0	0.23317
Left PrG precentral gyrus	-1.27245	23.2786	0	0.23342
Right PT planum temporale	-7.95868	5.77427	-0.08165	0.18999
Left PT planum temporale	-13.6171	0.3216	-0.16147	0
Right SCA subcallosal area	12.1687	3.36894	0.02896	0
Left SCA subcallosal area	11.271	1.70392	0.01615	0
Right SFG superior frontal gyrus	-0.74848	11.4176	0	0.19607
Left SFG superior frontal gyrus	-1.90879	11.9413	0	0.17828
Right SMC supplementary motor cortex	1.36407	2.92348	0	0
Left SMC supplementary motor cortex	0.28531	1.30349	0	0

Right SMG supramarginal gyrus	-47.9769	3.07503	-0.33785	0
Left SMG supramarginal gyrus	-60.9529	3.41068	-0.37277	0.10429
Right SOG superior occipital gyrus	-2.9757	0.45344	0	0
Left SOG superior occipital gyrus	-0.70766	3.84876	0	0.12067
Right SPL superior parietal lobule	-7.51241	1.52569	-0.17257	0
Left SPL superior parietal lobule	-12.5112	1.79292	-0.19693	0
Right STG superior temporal gyrus	-19.5533	0.52986	-0.18466	0
Left STG superior temporal gyrus	-14.7256	0.67456	-0.18506	0
Right TMP temporal pole	-47.7076	-21.6918	-0.28679	-0.12042
Left TMP temporal pole	-38.7424	-21.3961	-0.26189	-0.12065
Right TrIFG triangular part of the inferior frontal gyrus	0.86865	1.19197	0	0
Left TrIFG triangular part of the inferior frontal gyrus	0.33749	0.66059	0	0
Right TTG transverse temporal gyrus	-0.73044	0.83119	0	0
Left TTG transverse temporal gyrus	0.26298	0.05257	0	0

eTable 9: Clinical association studies for the cognitively unimpaired (CU) population from ADNI and BLSA. Each clinical variable/biomarker was fit with a linear regression model by controlling covariates. $-\log_{10}$(P-value) and the coefficient of each variable/biomarker (beta) are reported. For the P-values, we added the sign of the variable's beta coefficient values to indicate the effect's direction. The threshold for Bonferroni corrected $-\log_{10}$(P-value) is > 2.95. For the beta values, the ROIs that did not survive the multiple comparisons are assigned a value of 0.

Variable	R1: sign[$-\log_{10}$(P-value)]	R2: sign[$-\log_{10}$(P-value)]	R1: beta	R2: beta
FAQ_Total	0.03592	0.1324	0	0
CDR_Global	0.2549	0.68368	0	0
CDR_SOB	0.46167	0.38305	0	0
NPIQ_Total	-0.02945	-1.85116	0	0
DSST	0.79779	-0.17017	0	0
TMT_A	1.04091	0.26962	0	0
TMT_B	0.38981	1.39854	0	0
MMSE	-0.42715	-0.69585	0	0
Digit_Span_Backward	-1.11892	-0.4529	0	0
Digit_Span_Forward	-0.5489	0.15144	0	0
MOCA	-0.1209	0.046	0	0
BNT	0.18498	-0.7789	0	0
RAVLT	0.75931	-0.16779	0	0
RAVLT_IM	1.02925	0.03534	0	0
RAVLT_Short	0.41472	-0.42162	0	0
RAVLT_Long	0.35987	-0.51004	0	0
LM_DEL_A	0.05756	0.17738	0	0
LM_IM_A	-0.26376	0.45558	0	0
ANI_Fluency	0.07071	0.20993	0	0
VEG_Fluency	-0.02664	0.40168	0	0
TS_RATIO	1.86587	-0.00366	0	0
TS_RATIO_ADJ	1.97264	-0.12439	0	0
BNT_percent	0.18498	-0.7789	0	0
Cholesterol	-1.56606	-0.18187	0	0
Diastole	0.3944	-0.05256	0	0
Glucose	0.67578	-0.66702	0	0
Systole	0.84884	-0.22012	0	0
Triglycerides	-0.23883	-0.35205	0	0
ABETA42_ADNI	-0.15777	-0.07168	0	0
PTAU	-0.30024	1.00901	0	0
TAU	-0.29778	0.82113	0	0
Diabetes	1.08237	0.02205	0	0
Hypertension	-0.28435	-0.28563	0	0
Diagnosis_Depression	-0.59092	0.04985	0	0
Alcoholic	-0.22664	2.69173	0	0
Family_History_Dementia	-0.58766	0.17379	0	0
Ethnicity	1.44783	0.02901	0	0
Height	-0.01913	-0.29661	0	0
BMI	0.01531	-0.98463	0	0
Weight	0.01957	-0.95236	0	0
SPARE_AD	75.0432	138.158	0.12597	0.14245
SPARE_BA	14.9898	-3.16218	0.0059	-0.00218
AV45_PET_ADNI	0.42998	1.17676	0	0
FDG	0.58558	-1.02347	0	0
WMLS_Volume_701	6.92099	1.98594	5.70E-06	0

References

1. Yang, Z., Wen, J. & Davatzikos, C. Surreal-GAN:Semi-Supervised Representation Learning via GAN for uncovering heterogeneous disease-related imaging patterns. *ICLR* (2021).
2. Yang, Z. *et al.* A deep learning framework identifies dimensional representations of Alzheimer's Disease from brain structure. *Nat Commun* **12**, 7065 (2021).
3. Dong, A., Honnorat, N., Gaonkar, B. & Davatzikos, C. CHIMERA: Clustering of Heterogeneous Disease Effects via Distribution Matching of Imaging Patterns. *IEEE Trans. Med. Imaging* **35**, 612–621 (2016).
4. Varol, E., Sotiras, A. & Davatzikos, C. HYDRA: Revealing heterogeneity of imaging and genetic patterns through a multiple max-margin discriminative analysis framework. *NeuroImage* **145**, 346–364 (2017).
5. Wen, J. *et al.* Multi-scale semi-supervised clustering of brain images: Deriving disease subtypes. *Med Image Anal* **75**, 102304 (2021).
6. Wen, J. *et al.* Subtyping brain diseases from imaging data. Preprint at https://doi.org/10.48550/arXiv.2202.10945 (2022).
7. Young, A. L. *et al.* Uncovering the heterogeneity and temporal complexity of neurodegenerative diseases with Subtype and Stage Inference. *Nat Commun* **9**, 4273 (2018).
8. Petersen, R. C. *et al.* Alzheimer's Disease Neuroimaging Initiative (ADNI): clinical characterization. *Neurology* **74**, 201–209 (2010).
9. Resnick, S. M. *et al.* One-year age changes in MRI brain volumes in older adults. *Cereb Cortex* **10**, 464–472 (2000).
10. Miller, K. L. *et al.* Multimodal population brain imaging in the UK Biobank prospective epidemiological study. *Nat Neurosci* **19**, 1523–1536 (2016).

11. Watanabe, K., Taskesen, E., van Bochoven, A. & Posthuma, D. Functional mapping and annotation of genetic associations with FUMA. *Nat Commun* **8**, 1826 (2017).

12. Yang, J. *et al.* FTO genotype is associated with phenotypic variability of body mass index. *Nature* **490**, 267–272 (2012).

13. Choi, S. W., Mak, T. S.-H. & O'Reilly, P. F. Tutorial: a guide to performing polygenic risk score analyses. *Nat Protoc* **15**, 2759–2772 (2020).